Strathprints Institutional Repository

Colombo, Camilla and Xu, Ming and McInnes, Colin (2012) *Stabilisation of the hyperbolic equilibrium of high area-to-mass spacecraft.* In: 63rd International Astronautical Congress, 2012-10-01 - 2012-10-05, Naples.

http://strathprints.strath.ac.uk/

IAC-12.C1.1.13

STABILISATION OF THE HYPERBOLIC EQUILIBRIUM OF HIGH AREA-TO-MASS SPACECRAFT

Camilla Colombo[1], Ming Xu[2], Colin R. McInnes[3]

[1]Astronautics Group, University of Southampton, Southampton, United Kingdom
c.colombo@soton.ac.uk
[2] Dept. of Aerospace Engineering, School of Astronuatics, Beihang University, Beijing, China
xuming@buaa.edu.cn
[3]Advanced Space Concepts Laboratory, University of Strathclyde, Glasgow, United Kingdom
colin.mcinnes@strath.ac.uk

In this paper we propose the exploitation of anti-heliotropic orbits, corresponding to the hyperbolic solution of the J_2 and solar radiation pressure dynamical system, as gateway orbits between the low-eccentricity orbits where atmospheric drag does not affect the motion and the high eccentricity orbits which enter in drag regime. The eccentricity can be maintained in the neighborhood of the unstable point by means of a controller preserving the Hamiltonian structure of the system. In this way, any initial eccentricity close to the equilibrium conditions will lead to a bound trajectory around the controlled elliptic equilibrium. By selecting the time the controller is turned off, one of the two unstable manifolds leaving the equilibrium point can be followed, leading the orbit to become circular of to increase its eccentricity until natural decay occurs.

I. INTRODUCTION

The orbital evolution of high area-to-mass spacecraft, such as large thin solar sails or centimetre scaled 'smart dust' spacecraft [1], show a peculiar behaviour under the coupled effect of solar radiation pressure and the perturbation due to the Earth's oblateness. Long-term oscillations in eccentricity have been observed since 1960 in the orbital behaviour of satellites such as the ECHO balloon [2], Vanguard [3] and many others [4]. This dynamical system at low inclinations can be described through a Hamiltonian written in two variables, the osculating orbit eccentricity and the solar angle ϕ between the orbit pericentre and the Sun-line [5, 6]. At specific values of the orbit energy, the system allows the existence of three stationary points, of which two stable points at $\phi = 0$ and $\phi = \pi$ correspond respectively to

families of heliotropic and anti-heliotropic orbits [7]. The other stationary point correspond to a saddle solution.

The use of an anti-heliotropic elliptical orbit, corresponding to the stable equilibrium at $\phi = \pi$, has been proposed for the GeoSail mission as long residence times are spent in the geomagnetic tail, hence enabling the statistical characterisation of plasma under a variety of solar wind conditions [8, 9]. The spacecraft is injected into an elliptical orbit at the frozen eccentricity with a perigee of 10 Earth radii and apogee beyond 25 Earth radii. A passively stabilised sail is used to achieve the passive progression of the apsides line, synchronously with the Sun-Earth line. This orbit can be maintained for an indefinite time.

For lower values of semi-major axis, another equilibrium point exists in the phase space at $\phi = \pi$, due to the interaction with solar radiation pressure and the effect of the Earth's oblateness. This solution exists

within a relatively limited range of semi-major axis and eccentricities. For an object with a non-negligible area-to-mass, the hyperbolic equilibrium is found at high eccentricities and, interestingly, is very close to the critical eccentricity, for which the orbit perigee is within the Earth's atmosphere.

In this paper we propose the exploitation of anti-heliotropic orbits, corresponding to the hyperbolic solution of the dynamical system, as gateway orbits between the low-eccentricity orbits where atmospheric drag does not affect the motion and the high eccentricity orbits which enter in drag regime.

This unstable equilibrium has two dimensional stable and unstable manifolds of topological type 'saddle × saddle' in the phase space of eccentricity-ϕ. Therefore, the eccentricity cannot be maintained near this interesting equilibrium point unless a controller preserving the Hamiltonian structure is constructed to change its topological type from hyperbolic to elliptic [10]. In this way, any initial eccentricity close to equilibrium conditions will lead to a bound trajectory around the controlled elliptic equilibrium. The controller works well because the invariant manifolds are employed in a feedback to remove the unstable dynamics, which has potential applications in generating the bounded Lissajous orbits near the off-axis solar sail equilibrium in the sail's circular restricted three body problem [10], and quasi-periodic relative trajectories on a J_2-perturbed mean circular orbit [11].

The control for the hyperbolic point can then be exploited as a gateway from the low-eccentricity region where librational motion around the stable equilibria is possible, to the high-eccentricity region, where the spacecraft naturally decay due to atmospheric drag.

A GeoSail-type mission for the study of the close geomagnetic tail is designed, where a swarm of micro-spacecraft equipped with small solar sails is initially deployed on a circular orbit. The controller allows the stabilisation of the swarm on an anti-heliotropic elliptical orbits in correspondence to the hyperbolic equilibrium. Afterwards, at the end of life, the swarm is forced to orbit decay through the unstable manifold leading to high eccentricities an so lowering the orbit perigee.

This particular mission analysis is also envisaged to enhance coverage of the night side of a planet, for reflection of solar power, by passively transferring the spacecraft from a circular orbit, into an elliptical orbit, and then opening the "gateway to decay" at the end of mission or for a controlled decay about an oblate planet.

The control requirements are quantified for different solar sail requirements and spacecraft masses. It is sought that such a control can be given by controlling the attitude of the sail or through electro-chromic control [12].

II. PLANAR MODEL OF THE ORBITAL DYNAMICS

II.I. Simplified planar dynamics

The two-body dynamics of a spacecraft with high area-to-mass ratio orbiting the Earth is strongly perturbed by the term of the gravitational field due to the Earth's oblateness J_2 and by the effect of solar radiation pressure. The secular rate of the orbital elements due to SRP and J_2 can be written in polar coordinates of the eccentricity vector $\mathbf{e} = \begin{bmatrix} e_x, e_y \end{bmatrix}^T$:

$$\frac{de_x}{d\lambda_{\text{Sun}}} = e_y \left(1 - \frac{W}{\left(1 - e_x^2 - e_y^2 \right)^2} \right)$$

$$\frac{de_y}{d\lambda_{\text{Sun}}} = -C\sqrt{1 - e_x^2 - e_y^2} - e_x \left(1 - \frac{W}{\left(1 - e_x^2 - e_y^2 \right)^2} \right) \tag{1}$$

where $e_x = e\cos\phi$, $e_y = e\sin\phi$ [13], with e the eccentricity, and ϕ the angle between the Sun-Earth line and the direction of the orbit pericentre ($\phi = \tilde{\omega} - (\lambda_{\text{Sun}} - \pi)$ where $\tilde{\omega}$ defines the longitude of the

pericentre and λ_{Sun} the true longitude of the Sun), as shown in Fig. 1.
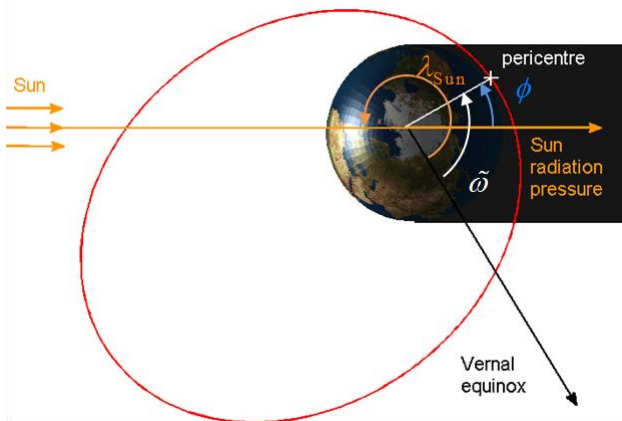
Fig. 1:   Planar orbit geometry.

Note that Eqs. (1) consider a planar problem only, i.e. the orbit has zero inclination and the equatorial plane is assumed to be in the ecliptic (i.e., the obliquity angle of the ecliptic with respect to the equator is set to zero). Moreover, the effect of the eclipses is neglected. As a consequence, the secular variation of semi-major axis and inclination is zero. These equations are governed by the solar radiation pressure parameter C and the oblateness parameter W, both dependent on the semi-major axis a

$$C = \frac{3}{2} a_{\text{SRP}} \frac{a^2}{\mu_{\text{Earth}}} \frac{n}{n_{\text{Sun}}}$$
$$W = \frac{3}{2} J_2 \frac{R_{\text{Earth}}^2}{a^2} \frac{n}{n_{\text{Sun}}} \qquad (2)$$

where a_{SRP} is the characteristic acceleration due to SRP $a_{\text{SRP}} = p_{\text{SR}} c_R A_{\text{Sun}} / m$ with $p_{\text{SR}} = 4.56 \times 10^{-6} \, \text{N/m}^2$ the solar pressure at 1 AU, c_R the reflectivity coefficient, taken equal to 1.8 in this paper, A_{Sun} is the area exposed to the Sun, and m is the mass of the body. In the expression for the oblateness parameter W $J_2 = 1.083 \cdot 10^{-3}$ denotes the second zonal harmonic coefficient and R_{Earth} is the mean radius of the Earth. n_{Sun} is the orbital angular velocity of the Earth around the Sun

(circular Earth orbit is adopted), $n = \sqrt{\mu_{\text{Earth}} / a^3}$ is the orbit angular velocity of the body on its orbit, where μ_{Earth} the gravitational constant of the Earth.

II.II. *Hyperbolic equilibrium*
As detailed in [7], Eqs. (1) allow as an integral of motion the Hamiltonian which is fixed by the initial condition of the integration:

$$H = -\sqrt{1 - e_x^2 - e_y^2} + C e_x - \frac{W}{3\left(1 - e_x^2 - e_y^2\right)^{3/2}} \qquad (3)$$

Eq. (3) describes the particle's trajectory in the e_x-e_y phase space as analysed by Hamilton and Krivov [14] and Krivov and Getino [6]. The Hamiltonian in Eq. (3) allows a maximum of three stationary points

The equilibrium of the 2-dimensional Hamiltonian system can be solved from:

$$\frac{\partial H}{\partial \mathbf{e}} = 0 \qquad (4)$$

We are now interested in the hyperbolic (saddle) equilibrium, which corresponds to the condition

$$H_{e_x e_x} \cdot H_{e_y e_y} - H_{e_x e_y}^2 < 0 \qquad (5)$$

The existence of the saddle and its eccentricity depends on the orbit semi-major axis and the area-to-mass of the spacecraft, which determines the SRP and J_2 parameters C and W in Eqs. (2). Fig. 2 from Ref. [7] shows the evolution of the eccentricity of the $\phi = 0$ and $\phi = \pi$ stationary points as function of the semi-major axis for different area-to-mass ratios and considering a reflectivity coefficient of 1.8. The eccentricity and semi-major axis range for which Eq. (5) is satisfied corresponds to the region in the graph between the black lines. The black line on the left boundary represents the solution for a Sun-synchronous orbit when the effect of SRP is negligible (i.e., conventional spacecraft for which we can assume $C = 0$), [14] and, unlike the J_2+SRP case, can be

achieved at any orientation of the orbit apse-line with respect to the Sun:

$$e_{\phi\text{-syn } J_2} = \sqrt{1 - \sqrt{W}} \qquad (6)$$

where the dependence on the semi-major axis is in the parameter W.

In correspondence of the black line at the right boundary, instead, the stable equilibrium at $\phi = \pi$ and the

saddle at $\phi = \pi$ converge to the same eccentricity in correspondence of a specific semi-major axis and area-to-mass ratio (coloured circle). The corresponding phase space is represented in Fig. 3.
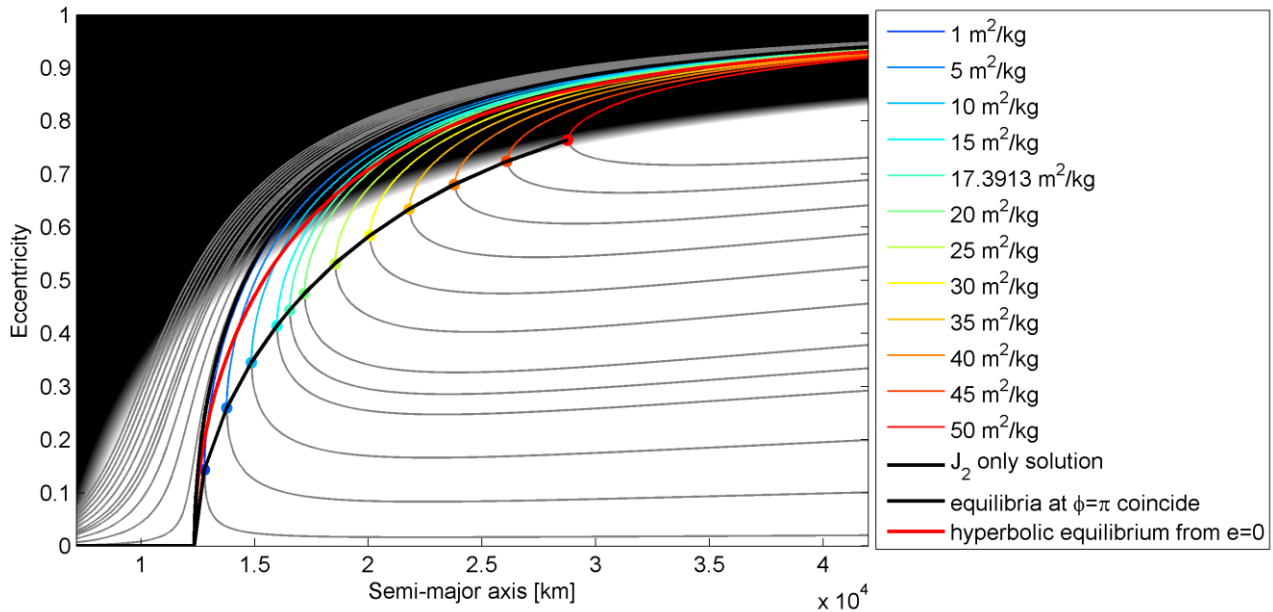
Fig. 2: Eccentricity and semi-major axis of the hyperbolic point for different area-to-mass ratios. The other stationary points of the system are plotted in grey. The black line on the left represents the sun-synchronous solution with J_2 only, the black line on the right represents the case in which the hyperbolic equilibrium and the stable equilibrium at $\phi=\pi$ coincide. The red line corresponds to sets of semi-major axis, eccentricities and area-to-mass ratios for which the Hamiltonian line passing through $e=0$ passes also through the hyperbolic eccentricity. The black shaded area represents orbits with a perigee below 800 km.
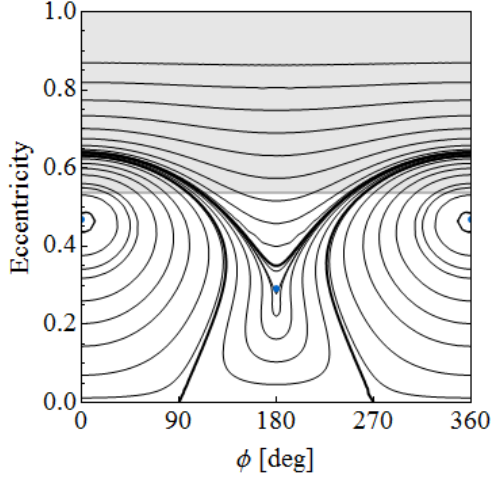
Fig. 3: Eccentricity-ϕ phase space evolution under the effects of J_2+SRP. The hyperbolic equilibrium point and the stable equilibrium point at $\phi=\pi$ coincide. Semi-major axis of 13,767 km and area-to-mass of 5 m2/kg.
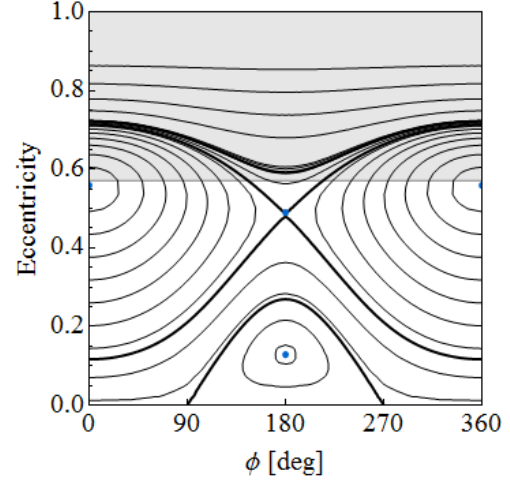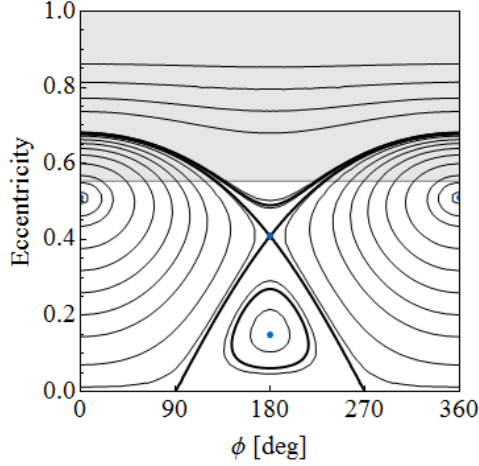

Fig. 4: Hyperbolic regime in the eccentricity-ϕ phase space evolution under the effects of J_2+SRP. The bold lines represent the separatrices in correspondence of the saddle point and zero eccentricity Hamiltonian, the shaded area marks orbit altitude lower than one Earth radius. Semi-major axis of 14,864 km and area-to-mass of 5 m²/kg.

Fig. 4 shows a typical phase space in the presence of an hyperbolic solution at eccentricity of 0.49 and $\phi = \pi$. The stable equilibria at $\phi = 0$ and $\phi = \pi$ are visible with an eccentricity of approximately 0.56 and 0.13, respectively. The evolution of initial conditions chosen in the neighbourhood of a stable equilibrium point will exhibit a librational evolution in the phase space around the stable equilibrium. The line generating in correspondence of $e = 0$ and $\phi = 2/3\pi$ separates the librational motion between the librational motion around $\phi = 0$ from a rotational evolution above. Note that not all values of eccentricity are feasible for a given semi-major axis a, since the orbit perigee cannot move within the atmosphere to keep the orbit stable. Hence, the eccentricity cannot exceed its critical value:

$$e_{\text{crit}} = 1 - \frac{R_{\text{Earth}} + h_{p\,\text{drag}}}{a} \qquad (7)$$

where we set $h_{p\,\text{drag}} = 800\,\text{km}$.

The line passing through the hyperbolic point separates the librational motion around $\phi = \pi$ from a rotational motion above and below [5]. In correspondence of the red line in Fig. 2, the separatrix lines passing through $e = 0$ and the saddle point overlap, as shown in Fig. 5. Such a condition was studied by Lücking et al. [15] for determining the minimum area-to-mass to allow natural de-orbit through an inflatable balloon to enhance the effect of solar radiation pressure. We will refer to the eccentricity of the hyperbolic point that can be reached from $e = 0$ as $e_{\text{hyp 0}}$. The reader can refer to Ref. [15] for the details on how to compute $e_{\text{hyp 0}}$ whose expression is also reported in the Appendix Section VI. Note that $e_{\text{hyp 0}}$ depends only on W in Eq. (2). However, for a certain semi-major axis, the value of $e_{\text{hyp 0}}$ can be achieved with a specific area-to-mass ratio, as visible from Fig. 2.

Fig. 5: **Hyperbolic regime in the eccentricity-ϕ phase space evolution under the effects of J_2+SRP. The separatrices in correspondence of the saddle point and zero eccentricity Hamiltonian coincide. Semimajor axis of 14,270.8 km and area-to-mass of 5 m^2/kg.**

III. STRUCTURE-PRESERVING STABILISATION FOR HAMILTONIAN SYSTEM

Most classical astrodynamics problems can be classified as Hamiltonian systems, e.g. the circular restricted three-body problem (CR3BP) [10], and the relative dynamics on a J_2-perturbed mean circular orbit [11]. For a hyperbolic Hamiltonian system, there exist hyperbolic equilibria that have stable, unstable, and centre manifolds, similar to the collinear libration points L_1, L_2, and L_3 in the CR3BP. The unstable manifolds will lead to instability. Bounded motions near hyperbolic equilibria have been broadly applied to various missions, such as missions to increase the coverage rate of an object (i.e., a ground station or target spacecraft), e.g. to explore of far-side of the Moon by using a s/c on the Lissajous orbit at the lunar L$_2$ point, and mission that avoid communication signals being lost in the Sun (e.g., SOHO spacecraft located at an halo orbit at Earth L$_1$ point), or to employ quasi-periodic relative trajectories for on-orbit surveillance, inspection or repair, which requires rapid changes in formation configuration for full three-dimensional imaging.

III.I. Controller design

A structure-preserving controller [10] is here proposed to generate bounded trajectories near the equilibrium for the time-independent planar Hamiltonian system Eq (1). The poles of the system can be assigned to any different positions on the imaginary axis by the controller, so that the topology type of the equilibrium is changed by the controller from hyperbolic (saddle) to elliptic (centre). According to the Morse lemma [16], higher-order nonlinear terms will bring stability in the controlled Hamiltonian system, so the controller is Lyapunov stable [17].

The controller feedbacks the difference between the actual locations and the equilibrium, so all the components of the controlled variables should be of the same type. Thus, the eccentricity vector $\mathbf{e} = \begin{bmatrix} e_x, e_y \end{bmatrix}^T$ is preferred to design the controller in this paper.

The hyperbolic equilibrium $\mathbf{e}_{hyp} = \begin{bmatrix} e_{x\,hyp}, e_{y\,hyp} \end{bmatrix}^T$ of the 2-dimensional Hamiltonian system is solved through Eqs. (4) and (5), and the variation equation Eq. (1) can be linearised near the equilibrium as:

$$\frac{d\tilde{\mathbf{e}}}{d\lambda_{Sun}} = \begin{bmatrix} \dfrac{\partial f_{e_x}}{\partial e_x} & \dfrac{\partial f_{e_x}}{\partial e_y} \\[2mm] \dfrac{\partial f_{e_y}}{\partial e_x} & \dfrac{\partial f_{e_x}}{\partial e_y} \end{bmatrix} \begin{bmatrix} e_x - e_{x\,hyp} \\ e_y - e_{y\,hyp} \end{bmatrix} \tag{8}$$

For the hyperbolic system, the hyperbolic eigenvalues of the matrix associated to the system Eq. (8) are denoted as $\pm\sigma$, and the stable\unstable manifolds are denoted as $\mathbf{u}_\pm$. Then the controller is constructed as follows:

$$\mathbf{T} = -\sigma^2 \begin{bmatrix} G_1 \mathbf{u}_+ \mathbf{u}_+^T + G_2 \mathbf{u}_- \mathbf{u}_-^T \end{bmatrix} \cdot \left(\mathbf{e} - \mathbf{e}_{hyp} \right) \tag{9}$$

where G_1 and G_2 are the controller gains of the unstable and stable manifolds, respectively.

Some propositions and theorems have been put forward for the two-dimensional Hamiltonian system [10]. The stable and unstable manifolds can be used to

stabilize the system with different gains, however if one of the gains G_1 or G_2 is zero, this will lead to the failure of the stabilisation.

III.II. Application of Hamiltonian structure-preserving control to stabilise relative motions about the hyperbolic eccentricity

In the phase space represented in Fig. 4, the hyperbolic eccentricity located at $\phi = \pi$ is unstable, and its invariant manifolds can be considered as the separatrix of the Hill's regions defined by the other stable equilibrium points of system Eq. (3). Therefore, any spacecraft near the hyperbolic eccentricity cannot be maintained on such an orbit; rather, depending on very small change in the orbital elements, it will move on the unstable manifold towards higher eccentricities, or on the unstable manifold towards lower eccentricities. By applying the Hamiltonian structure-preserving controller in Eq. (9), bounded trajectories can be achieved in the phase space near the hyperbolic eccentricity, like the one shown with the red line in Fig. 6. Differently to second-order dynamical systems (such as the CR3BP), only periodic trajectories can be generated by the controller, because any intersection between the identical flow of the first-order Hamiltonian system is prohibited.
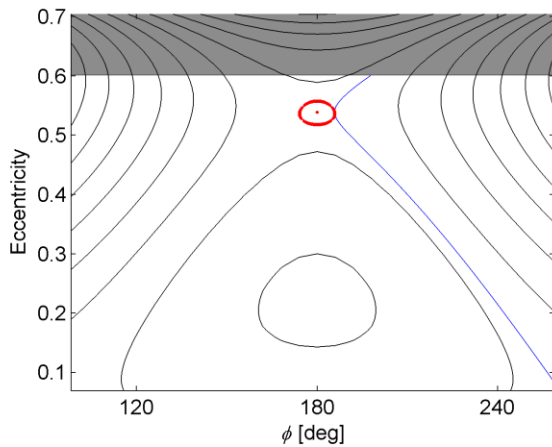
Fig. 6: Controlled eccentricity near the hyperbolic point. The red solid line represents the periodic trajectory of the controlled eccentricity, and the blue line represents the natural trajectory of the uncontrolled eccentricity which reaches and then leaves the hyperbolic equilibrium.

The proposed controller has potential applications into holding the spacecraft near the hyperbolic eccentricity during the mission life. At the end-of-life, the spacecraft can decide to decay (increasing its eccentricity beyond than the critical one Eq. (7)) or to return to the circular orbit.

IV. MISSION DESIGN

A spacecraft is initially placed into a 15,973 km circular orbit. When the solar sail is deployed, the A/m of the spacecraft increases from 0.01 to 10 m^2/kg. Therefore, the orbit eccentricity will naturally increase, following the blue line in Fig. 2. The value of the semi-major axis was selected so that the hyperbolic eccentricities, equal to 0.5383, can be reached from a circular orbit (i.e., intersection of the red line with the 10 m^2/kg light line in Fig. 2). At the hyperbolic point the control gains are set to $G_+=2$, and $G_-=-2$ and the red trajectory is obtained. By applying the control, the phase space position can be stabilised indefinitely. This orbit corresponds to an anti-heliotropic highly elliptical orbit, which maintains its apogee in the direction opposite to the Sun. Such an orbit can be exploited for mapping the phenomena in the close magnetic tail of the Earth as the apogee is always at 18,193 km behind the Earth. Another application of such orbits can be envisaged for transmitting data or power (in this case a small inclination would be needed to free the spacecraft from eclipses at the apogee). In fact, the spacecraft will dwell on the night side of the Earth for a higher fraction of its period.

Depending on the timing, the controller is turned off, the spacecraft can either go back to circular orbit (see Fig.

7 in Section IV.I), or continue on the phase line used for reaching the hyperbolic equilibrium and naturally move to higher eccentricities (see Fig. 11 in Section IV.II), where the effect of drag will cause the de-orbit and re-entry.

IV.I. Gateway to circular orbits

The mission in Fig. 7 is composed by three phases: (1) transfer from circular orbit to the hyperbolic equilibrium, represented by the blue line, (2) stabilisation around the hyperbolic equilibrium (red line) and (3) transfer back to circular orbit represented by the dotted blue line. At the hyperbolic eccentricity the orbit is maintained by the controller for a period of five years, as shown in Fig. 8 and Fig. 9.
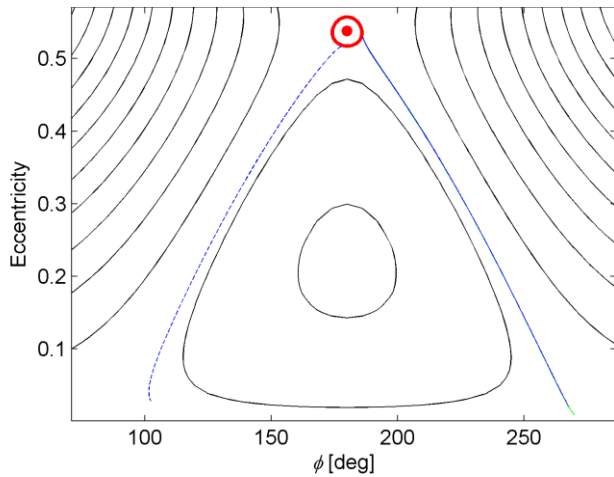
Fig. 7: Hyperbolic point as gateway to circular orbit. Phase 1: transfer from circular orbit to the hyperbolic equilibrium (blue line); phase 2: stabilisation around the hyperbolic equilibrium (red line) and phase 3: transfer back to circular orbit represented by the dotted blue line. The major semi-axis is 15,973 km, and the area-to-mass ratio is 10 m² /kg.
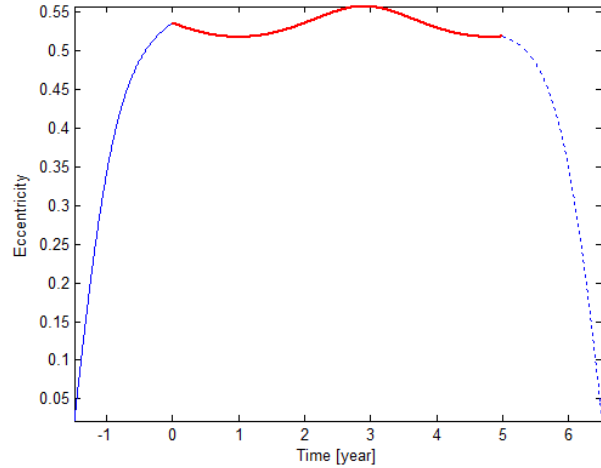

Fig. 8: History of the eccentricity during the mission. The red solid line represents the periodic trajectory of the controlled eccentricity, and the blue solid and dotted lines represent the initial and final natural trajectory of the uncontrolled eccentricity. The major semi-axis is 15,973 km, and the area-to-mass ratio is 10 m² /kg.
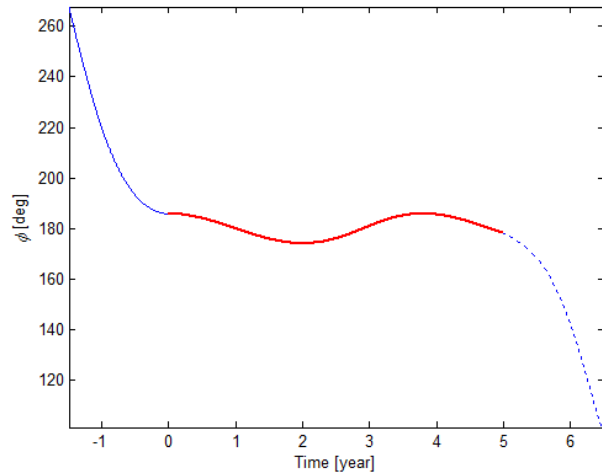

Fig. 9: History of ϕ during the mission. The red solid line represents the periodic trajectory of the controlled eccentricity, and the blue solid and dotted lines represent the initial and final natural trajectory of the uncontrolled eccentricity. The major semi-axis is 15,973 km, and the area-to-mass ratio is 10 m² /kg.

Fig. 10 gives the magnitude of the control acceleration during the mission.
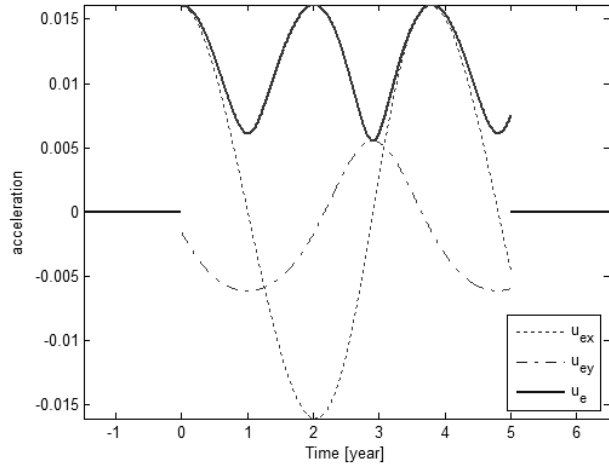
Fig. 10: The history of acceleration during the mission. The solid line represents the magnitude of control acceleration, and the dotted lines represents the control on e_x, and the dash-dotted lines represents the control on e_y. The major semi-axis is 15,973 km, and the area-to-mass ratio is 10 m^2/kg.
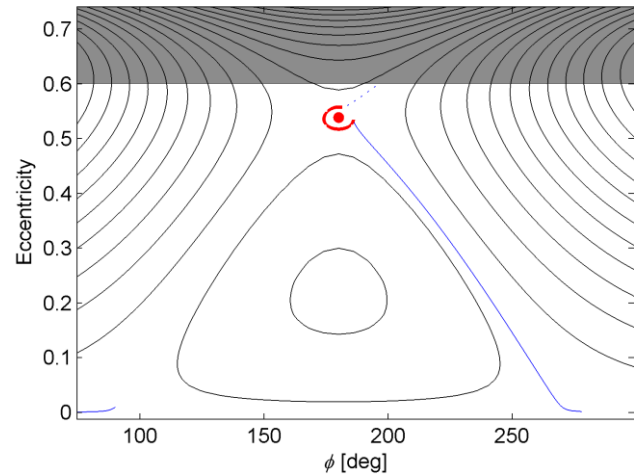

Fig. 11: Hyperbolic point as gateway to highly-elliptical orbits orbit. Phase 1: transfer from circular orbit to the hyperbolic equilibrium (blue line); phase 2: stabilisation around the hyperbolic equilibrium (red line) and phase 3: transfer beyond the critical eccentricity represented by the dotted blue line. The major semi-axis is 15,973 km, and the area-to-mass ratio is 10 m^2/kg.

IV.II. Gateway to highly-elliptical orbits

After the stabilisation phase at the hyperbolic point with the control gains G_+=2, and G_-=-2 the mission can evolve also in a different way. As it is shown in Fig. 11 the spacecraft can decide to leave the eccentricity point following the unstable manifold towards higher eccentricities end enters the planet atmosphere, when the orbit will naturally decay. The mission in Fig. 11 is composed by three phases: (1) transfer from circular orbit to the hyperbolic equilibrium, represented by the blue line, (2) stabilisation around the hyperbolic equilibrium (red line) and (3) transfer beyond the critical eccentricity represented by the dotted blue line. At the hyperbolic eccentricity the orbit is maintained by the controller for a period of three years, as shown in Fig. 12 and Fig. 13. The magnitude of the control acceleration during the mission (see Fig. 14) has the same profile as in Fig. 10, the only difference is that the time for which the spacecraft is stabilised is here reduced to three years in order to meet the unstable manifold towards high eccentricities.
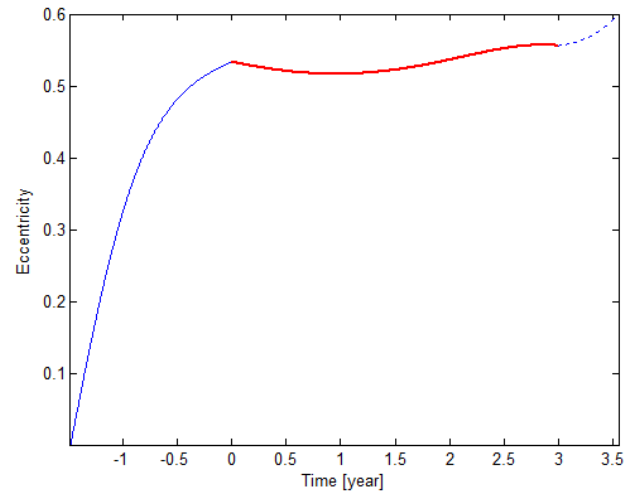
Fig. 12: History of the eccentricity during the mission. The red solid line represents the periodic trajectory of the controlled eccentricity, and the blue solid and dotted lines represent the initial and final natural trajectory of the uncontrolled eccentricity. The major semi-axis is 15,973 km, and the area-to-mass ratio is 10 m^2/kg.
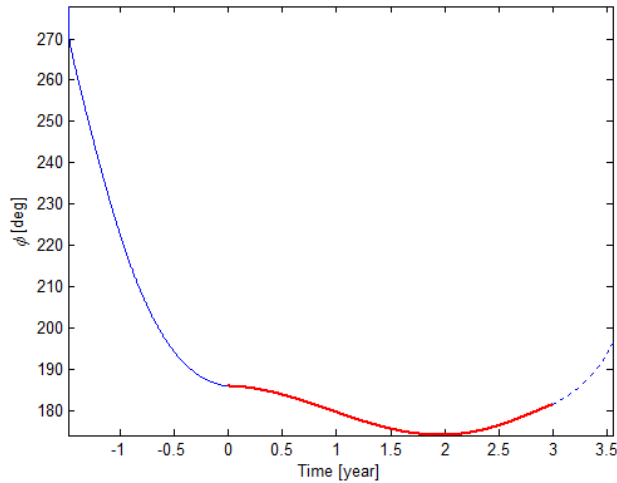
Fig. 13: History of ϕ during the mission. The red solid line represents the periodic trajectory of the controlled eccentricity, and the blue solid and dotted lines represent the initial and final natural trajectory of the uncontrolled eccentricity. The major semi-axis is 15,973 km, and the area-to-mass ratio is 10 m^2/kg.
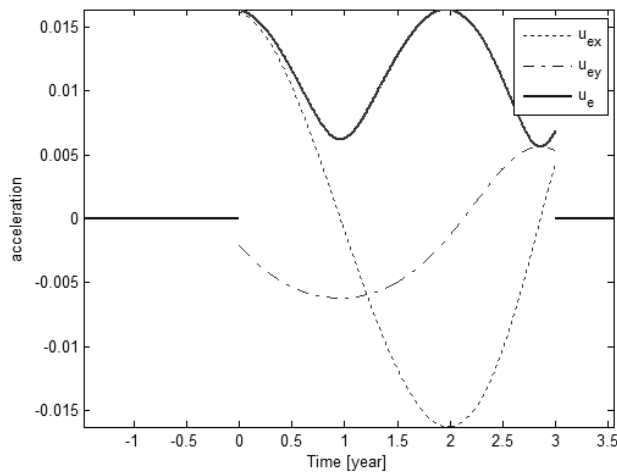

Fig. 14: The history of acceleration during the mission. The solid line represents the magnitude of control acceleration, and the dotted lines represents the control on e_x, and the dash-dotted lines represents the control on e_y. The major semi-axis is 15,973 km, and the area-to-mass ratio is 10 m^2/kg.

IV.III. Gateway to circular orbits for short-term solar sail

A smaller solar sail is here considered so that the area-to-mass of the spacecraft is 5 m^2/kg. The mission leaves

from circular orbit with a semi-major axis of 14,275 km and reaches in less than two years the hyperbolic eccentricity equal to 0.4091 (phase 1). During phase 2 of the mission, which last 5 years, the eccentricity is maintained liberating about the stationary value, though the Hamiltonian-preserving controller, with gains set as G_+=3, and G_-=-3. Fig. 15, Fig. 16, Fig. 17 represents the mission evolution in terms of orbital elements, while Fig. 18 report the magnitude of the control acceleration. Note that the control acceleration reaches a lower peak when employing a lower A/m.
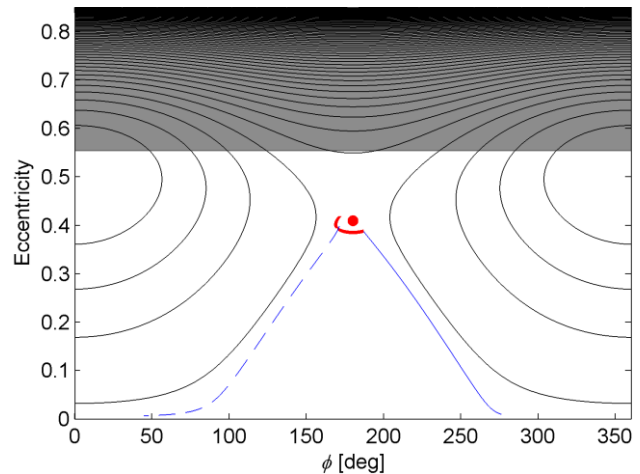

Fig. 15: Hyperbolic point as gateway to circular orbit. Phase 1: transfer from circular orbit to the hyperbolic equilibrium (blue line); phase 2: stabilisation around the hyperbolic equilibrium (red line) and phase 3: transfer back to circular orbit represented by the dotted blue line. The major semi-axis is 14,275 km, and the area-to-mass ratio is 5 m^2/kg.
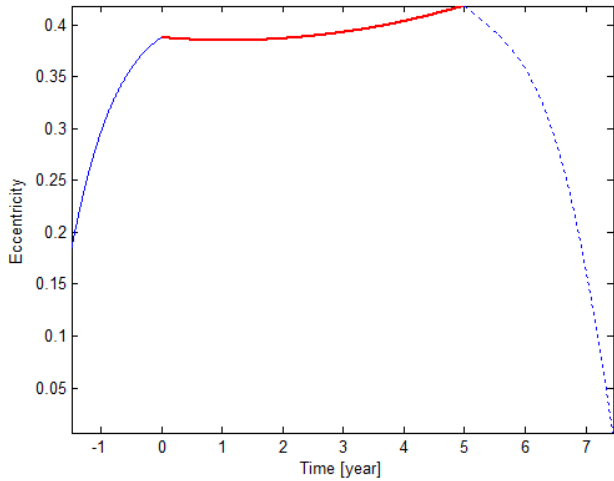
Fig. 16: History of the eccentricity during the mission. The red solid line represents the periodic trajectory of the controlled eccentricity, and the blue solid and dotted lines represent the initial and final natural trajectory of the uncontrolled eccentricity. The major semi-axis is 14,275 km, and the area-to-mass ratio is 5 m^2/kg.
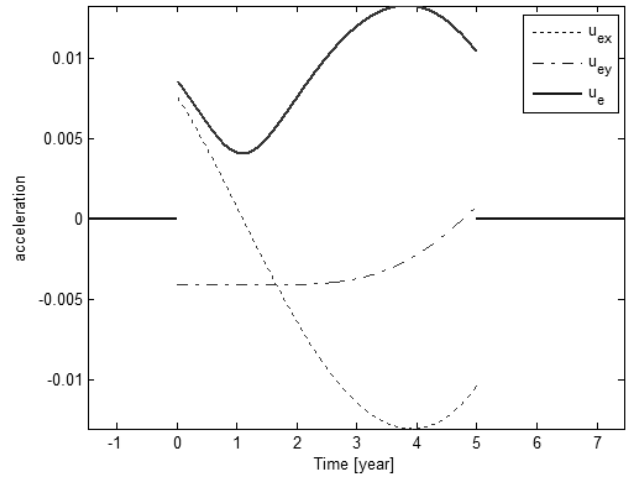

Fig. 18: The history of acceleration during the mission. The solid line represents the magnitude of control acceleration, and the dotted lines represents the control on e_x, and the dash-dotted lines represents the control on e_y. The major semi-axis is 14,275 km, and the area-to-mass ratio is 5 m^2/kg.
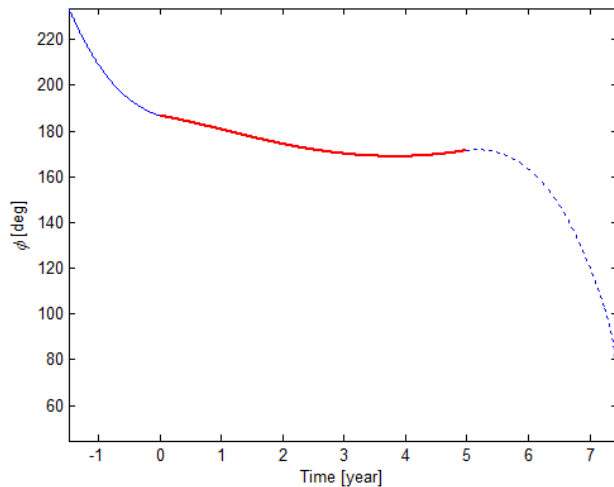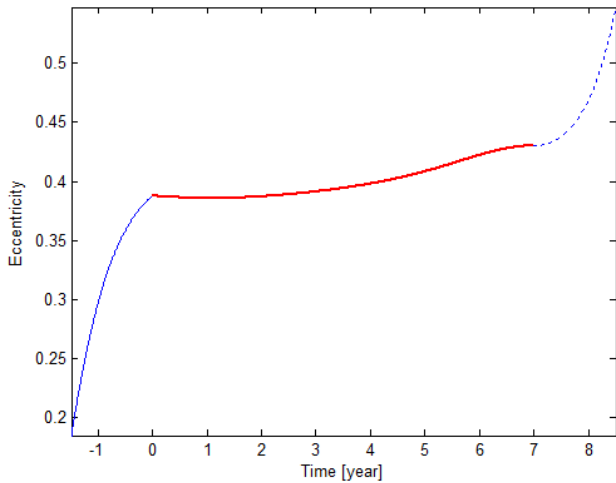

Fig. 17: History of ϕ during the mission. The red solid line represents the periodic trajectory of the controlled eccentricity, and the blue solid and dotted lines represent the initial and final natural trajectory of the uncontrolled eccentricity. The major semi-axis is 14,275 km, and the area-to-mass ratio is 5 m^2/kg.

IV.IV. Gateway to highly-elliptical orbits for short-term solar sail
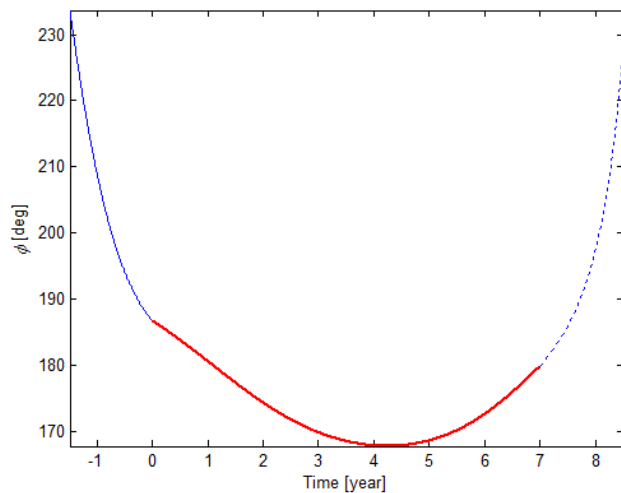
In the same way as before, the 3rd phase of the mission can be designed to reach to highly elliptical orbits, by properly selecting the time at which the controller is turned off, equal to seven years. The overall mission is represented in Fig. 19 to Fig. 22. Note that here the control gain were set to G_+=2.9, and G_-=-2.9.
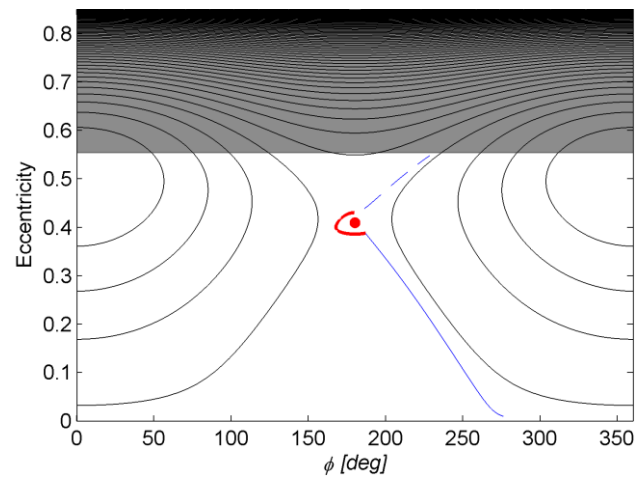
Fig. 19: Hyperbolic point as gateway to highly-elliptical orbits orbit. Phase 1: transfer from circular orbit to the hyperbolic equilibrium (blue line); phase 2: stabilisation around the hyperbolic equilibrium (red line) and phase 3: transfer beyond the critical eccentricity represented by the dotted blue line. The major semi-axis is 14,275 km, and the area-to-mass ratio is 5 m²/kg.

Fig. 21: History of ϕ during the mission. The red solid line represents the periodic trajectory of the controlled eccentricity, and the blue solid and dotted lines represent the initial and final natural trajectory of the uncontrolled eccentricity. The major semi-axis is 14,275 km, and the area-to-mass ratio is 5 m²/kg.

Fig. 20: History of the eccentricity during the mission. The red solid line represents the periodic trajectory of the controlled eccentricity, and the blue solid and dotted lines represent the initial and final natural trajectory of the uncontrolled eccentricity. The major semi-axis is 14,275 km, and the area-to-mass ratio is 5 m²/kg.
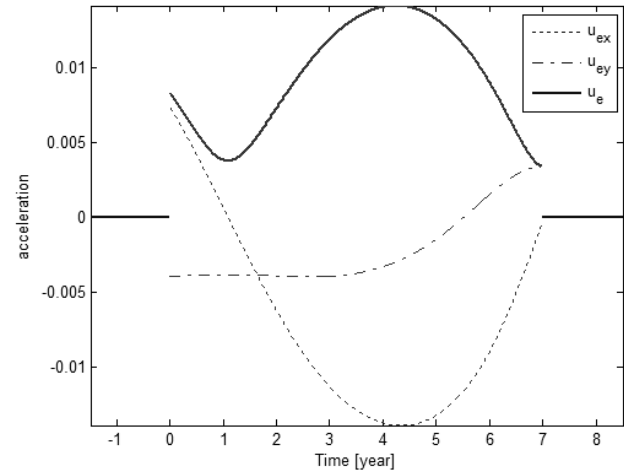
Fig. 22: The history of acceleration during the mission. The solid line represents the magnitude of control acceleration, and the dotted lines represents the control on e_x, and the dash-dotted lines represents the control on e_y. The major semi-axis is 14,275 km, and the area-to-mass ratio is 5 m²/kg.

IV.V. Gateway mission very small solar sail

The same mission scenario was run also for the case in which the spacecraft have an area-to-mass of 1 m²/kg. This case is very short-term mission, as for example a 100 kg spacecraft would require only a 5.6 m radius solar sail. The spacecraft is placed at a lower circular orbit with semi-major axis of 12,913 km. The hyperbolic eccentricity at 0.2278 can be maintained increasing the controller gains to G_+=9, and G_-=-9. This has an impact on the magnitude of the control acceleration, which increases to 0.02 km/s² (see Fig. 23). The required control can be given by the solar sail which can change its attitude at the hyperbolic point. Future work will be devoted to derive the control law as function of the true

anomaly along the orbit that can be translated into the secular acceleration u_{ex} and u_{ey}.
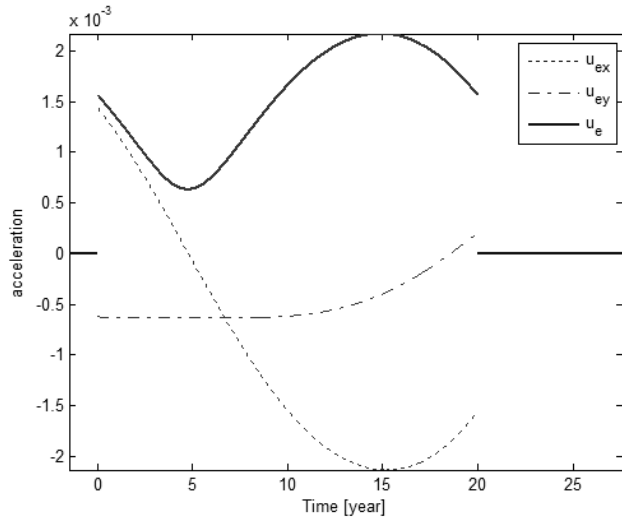

Fig. 23: The history of acceleration during the mission. The solid line represents the magnitude of control acceleration, and the dotted lines represents the control on e_x, and the dash-dotted lines represents the control on e_y. The major semi-axis is 12,913 km, and the area-to-mass ratio is 1 m^2/kg.

V. CONCLUSIONS

This paper considered the dynamics of a spacecraft with area-to-mass higher than 1 m^2/kg in the vicinity of the Earth or another planet. In particular, the attention was focused on the hyperbolic equilibrium point which exists for relatively low semi-major axis, due to the interaction of the Earth's oblateness with the secular effects of solar radiation pressure on a light weight reflective solar sail. A controller which preserves the Hamiltonian structure of the system was used for stabilising the orbits around the hyperbolic equilibrium point. If the semi-major axis is properly selected, the critical eccentricity can be naturally reached from a circular orbit, by following the line the $e-\phi$ phase space evolution. At the critical eccentricity, by selecting the time when the controller is turned off, the mission can evolve in two ways: either going back to zero eccentricity or following the other unstable manifold which will bring the spacecraft on a highly-elliptical orbit, where atmospheric drag will cause the perigee to decrease and the following re-entry. Such mission design has been proposed for several mission applications: for mapping the close magnetic tail of the Earth, or for stabilising a swarm of small spacecraft in the dark side of the planet for power and data transmission. The elliptical orbit at the critical eccentricity is always oriented with the apogee in the direction away of the Sun; therefore, the spacecraft will spend a longer fraction of its orbit in the night side of the Earth. The hyperbolic point can thus be transformed in a controlled gateway towards low eccentricity or high eccentricity orbits.

In a future work, the control requirements will be quantified for different mission durations and feasible control systems will be studied for stabilisation, relying on solar sail, low-thrust propulsion, or electro-chromic control. Also an analytical method to automatically select the time when the control is turned off will be defined.

VI. APPENDIX: HYPERBOLIC ECCENTRICITY FOR HAMILTONAIN LINE PASSING THROUGH e=0

The expression of the hyperbolic eccentricity in correspondence of the Hamiltonian line passing through $e = 0$ is [15]:

$$e_{\text{hyp }0} = \frac{1}{2}\left(5 - \frac{9}{(3+W)^2} - \left(\frac{2}{3}\left(-B - \frac{1}{(3+W)^6}\left(W(3+W)^2(18+5W)(-72+W(W-30))\right.\right.\right.$$

$$+\frac{1}{A}\left(4W^2(3+W^4)(648+7W(63+11W))\right)+2(3+W)^4 A - \frac{1}{B}\left(9W^2\left(1944+W(3240+W(1896+W(466+41W)))\right)\right)\Big)\Big)\Big)^{1/2}\Big)^{1/2}$$

where *A* and *B* are defined as:

$$A = \left(46656W^3 + 57469.5W^4 + 22707W^5 + 2903.5W^6 + 40.5\sqrt{3W^7(3+W)^2\left(20736+22779W+8218W^2+971W^3\right)}\right)^{1/3}$$

$$B = \sqrt{\frac{\left(36+30W+5W^2\right)^2}{(3+W)^4} + \frac{8W^2\left(648+441W+77W^2\right)}{3(3+W)^2 A} + \frac{4A-16\left(27+18W+5W^2\right)}{3(3+W)^2}}$$

VII. REFERENCES

[1] Colombo, C. and McInnes, C., "Orbital Dynamics of 'Smart Dust' Devices with Solar Radiation Pressure and Drag," *Journal of Guidance, Control, and Dynamics*, Vol. 34, No. 6, 2011, pp. 1613-1631. doi: 10.2514/1.52140

[2] Shapiro, I. I. and Jones, H. M., "Perturbations of the Orbit of the Echo Balloon," *Science*, Vol. 132, No. 3438, 1960, pp. 1484-1486. doi: 10.1126/science.132.3438.1484

[3] Musen, P., Bryant, R. and Bailie, A., "Perturbations in Perigee Height of Vanguard I," *Science*, Vol. 131, No. 3404, 1960, pp. 935-936. doi: 10.1126/science.131.3404.935

[4] Harwood, N. M. and Swinerd, G. G., "Long-Periodic and Secular Perturbations to the Orbits of Explorer 19 and Lageos Due to Direct Solar Radiation Pressure," *Celestial Mechanics and Dynamical Astronomy*, Vol. 62, No. 1, 1995, pp. 81-92. doi: 10.1007/BF00692070

[5] Hamilton, D. P., "Motion of Dust in a Planetary Magnetosphere: Orbit-Averaged Equations for Oblateness, Electromagnetic, and Radiation Forces with Application to Saturn's E Ring," *Icarus*, Vol. 101, No. 2, 1993, pp. 244-264. doi: DOI: 10.1006/icar.1993.1022

[6] Krivov, A. V. and Getino, J., "Orbital Evolution of High-Altitude Balloon Satellites," *Astron. Astrophys.*, No. 318, 1997, p. 7.

[7] Colombo, C., Lücking, C. and McInnes, C. R., "Orbital Dynamics of High Area-to-Mass Ratio Spacecraft with J2 and Solar Radiation Pressure for Novel Earth Observation and Communication Services," *Acta Astronautica*, Vol. 81, No. 1, 2012, pp. 137-150. doi: 10.1016/j.actaastro.2012.07.009

[8] McInnes, C. R., Macdonald, M., Angelopolous, V. and Alexander, D., "Geosail: Exploring the Geomagnetic Tail Using a Small Solar Sail," *Journal of Spacecraft and Rockets*, Vol. 38, No. 4, 2001, pp. 622-629.

[9] Oyama, T., Yamakawa, H. and Omura, Y., "Orbital Dynamics of Solar Sails for Geomagnetic Tail Exploration," *Journal of Guidance, Control and Dynamics*, Vol. 45, No. 2, 2008, pp. 316-323. doi: 10.2514/1.31274

[10] Xu, M. and Xu, S., "Structure-Preserving Stabilization for Hamiltonian System and Its Applications in Solar Sail," *Journal of Guidance, Control and Dynamics, accepted for publication*, Vol. 32, No. 3, 2009, pp. 997-1004.

[11] Xu, M., Zhu, J., Tan, T. and Xu, S., "Application of Hamiltonian Structure-Preserving Control to Formation Flying on a J2-Perturbed Mean Circular Orbit," *Celestial Mechanics and Dynamical Astronomy*, Vol. 113, No. 4, 2012, pp. 403-433.

[12] Lücking, C., Colombo, C. and McInnes, C., "Electrochromic Orbit Control for Smart-Dust Devices," *Journal of Guidance, Control and Dynamics, accepted for publication*, Vol. 35, No. 5, 2012, pp. 1548-1558. doi: 10.2514/1.55488

[13] Shapiro, B. E., "Phase Plane Analysis and Observed Frozen Orbit for the Topex/Poseidon Mission," *Sixth International Space Conference of Pacific Basin Societies*, Marina del Rey, CA, 1995.

[14] Hamilton, D. P. and Krivov, A. V., "Circumplanetary Dust Dynamics: Effects of Solar Gravity, Radiation Pressure, Planetary Oblateness, and Electromagnetism," *Icarus*, Vol. 123, No. 2, 1996, pp. 503-523. doi: 10.1006/icar.1996.0175

[15] Lücking, C., Colombo, C. and McInnes, C. R., "Solar Radiation Pressure-Augmented Deorbiting: Passive End-of-Life Disposal from High Altitude Orbits," *Journal of Guidance, Control and Dynamics*, Vol. currently under review, 2012.

[16] Golubitsky, M. and Marsden, J., "The Morse Lemma in Infinite Dimensions Via Singularity Theory," *SIAM J. Math. Anal.*, Vol. 14, No. 6, 1983, pp. 1037-1044.

[17] Wiggins S., *Introduction to Applied Nonlinear Dynamical Systems and Chaos, 2nd Ed.*, Springer–Verlag, New York, 2003, Ch. 19.